Continuous high-frequency turbulence and suspended sediment concentration measurements in an upper estuary

Mark Trevethan, Hubert Chanson*, Maiko Takeuchi

Divison of Civil Engineering, The University of Queensland, St Lucia, Brisbane, QLD 4072, Australia

Abstract

The present study details new turbulence field measurements conducted continuously at high frequency for 50 hours in the upper zone of a small subtropical estuary with semi-diurnal tides. Acoustic Doppler velocimetry was used, and the signal was post-processed thoroughly. The suspended sediment concentration wad further deduced from the acoustic backscatter intensity. The field data set demonstrated some unique flow features of the upstream estuarine zone, including some low-frequency longitudinal oscillations induced by internal and external resonance. A striking feature of the data set is the large fluctuations in all turbulence properties and suspended sediment concentration during the tidal cycle. This feature has been rarely documented.
© 2007 Elsevier Ltd. All rights reserved.

Keywords: turbulence measurements; suspended sediment concentration; subtropical estuary; continuous high-frequency sampling; acoustic backscatter

1. Introduction

In natural estuaries, the prediction of scalar dispersion can rarely be predicted analytically or numerically without exhaustive field data for calibration and validation. Why? In natural estuaries, the flow Reynolds number is typically within the range of $1\,E+5$ to $1\,E+8$ and more. The flow is turbulent, and we lack some fundamental understanding of the turbulence structure. A few studies investigated the lower and middle estuary regions, but the upper/upstream estuary dynamics received little attention.

The purpose of this study is to investigate thoroughly the turbulence and sediment suspension characteristics in the upper estuary zone of a small subtropical system with semi-diurnal tides. Detailed field measurements were conducted continuously at high frequency for 50 hours. The results yielded an unique series of continuous high-frequency long duration (50 Hz, 50 hours) measurements of turbulent velocity and suspended sediment concentration SSC in the upper estuary.

2. Turbulence in small estuaries

Turbulent flows have a great mixing potential involving a wide range of eddy length scales. Although the turbulence is a "random" process, the small departures from a Gaussian probability distribution are some of the key features of turbulence. The measured statistics should include the spatial distribution of turbulent stresses, the rates at which the individual stresses are produced, destroyed or transported from one point in space to another, the contribution of different sizes of eddy to the Reynolds stresses, and the contribution of different sizes of eddy to the turbulent production, dissipation and transport rates (Bradshaw, 1971). The turbulent Reynolds stress is a property of the flow. It is a transport effect resulting from turbulent motion induced by velocity fluctuations with its subsequent increase of momentum exchange and of mixing (Piquet, 1999).

---

* Corresponding author.

E-mail address: h.chanson@uq.edu.au (H. Chanson).

In natural waterways, the turbulence measurements must be conducted at high frequency to characterise the small eddies and the viscous dissipation process. They must also to be performed over a period significantly larger than the characteristic time of the largest vortical structures to capture the ''random'' nature of the flow and its deviations from Gaussian statistical properties. Turbulence is neither homogeneous nor isotropic. Altogether detailed turbulence measurements are almost impossible in estuarine flows unless continuous sampling at high frequency is performed. The estuarine conditions may vary significantly with the falling or rising tide. In small estuaries and inlets, the shape of the channel cross-section changes drastically with the tides as shown in Figs. 1 and 2. Fig. 1 illustrates the present sampling site at high and low tides, and the corresponding cross-section areas are shown in Fig. 2. Note the platform on the right bank for scale in Fig. 1.

All the requirements place some constraint on the selection of instrumentation for field deployment. Traditional propeller and electro-magnetic current meters are adequate for time-averaged velocity measurements, but they lack temporal and spatial resolution. One technique is the acoustic Doppler velocimetry (ADV) used herein, but it might adversely affected by ''spikes'', noise and disturbances (Goring and Nikora, 2002).

2.1. Field study and instrumentation

The field study was conducted in a small subtropical estuary of Eastern Australia with semi-diurnal tides. The estuarine zone is 3.8 km long, about 1 to 2 m deep mid-stream, and about 20–30 m wide. This is a relatively small estuary with a narrow, elongated and meandering channel, a cross-section which deepens and widens towards the mouth, surrounded by extensive mud flats, and some small, sporadic freshwater inflow. The catchment area is about 40 km^2. The estuary is a drowned river valley type with a wet and dry tropical/subtropical hydrology. This type of estuary accounts for nearly 30% of all estuaries of Australia (Digby et al., 1999).

Fig. 1. Photographs of the sampling site in the upper estuarine zone of Eprapah Creek. (A) High tide on 28 Aug. 2006 looking downstream (Courtesy of CIVL4120 student Group 3). (B) Low tide on 5 June 2006 looking downstream.
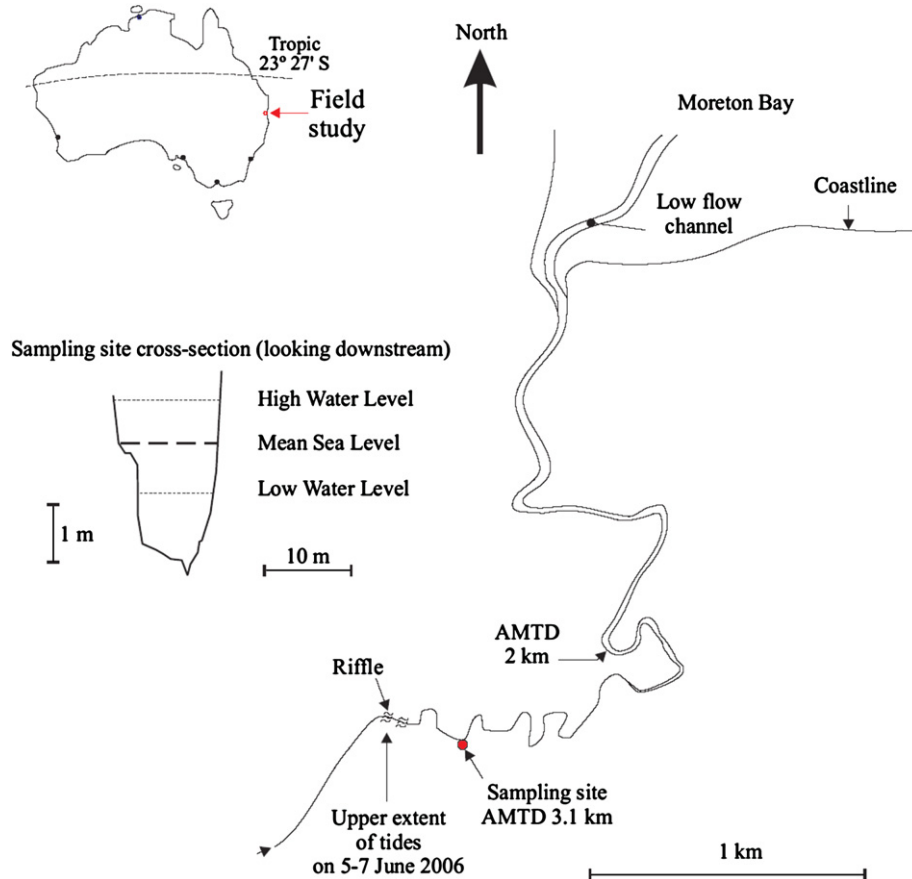
Fig. 2. Map of the estuarine zone of Eprapah Creek and cross-section at the sampling site (looking downstream) – The adopted middle thread distance (AMTD), measured from the river mouth, is indicated.

Although the tides are semi-diurnal, the tidal cycles have slightly different periods and amplitudes indicating some diurnal inequality. The estuary was previously investigated with a focus on the mid-estuarine zone (Chanson, 2003; Chanson et al., 2005a; Trevethan et al., 2006). New measurements were performed in the upstream zone at about 3.1 km from the river mouth on 5 to 7 June 2006 for 50 hours (Fig. 2). The maximum tidal range at the river mouth was 1.58 m corresponding to neap tidal conditions. At the sampling site, the measured water depth at the deepest section ranged from 1.11 m to 2.69 m, and the free-surface width from 9.2 to about 11 m during the field study (Figs. 1 and 2).

The study was conducted during dry weather conditions, and the freshwater runoff was zero (Fig. 3A). It was observed at the "riffles" which marked the upstream extent of the tides, sketched in Fig. 2. Fig. 3B illustrates the same site during a sporadic storm runoff six months earlier.

2.2. Instrumentation

Turbulent velocities were measured with an acoustic Doppler velocimeter Sontek 2D microADV (16 MHz). The measurements were performed continuously at 50 Hz for 50 hours. The sampling volume was located at 0.2 m above the bed and 4.2 m from the right bank. A thorough post-processing technique was developed and applied to remove electronic noise, physical disturbances and Doppler effects (Chanson et al., 2005b). The field experiences demonstrated that the "raw" ADV data were unsuitable, and often inaccurate in terms of time-averaged flow properties. Herein only post-processed data are discussed. In addition, some basic physio-chemistry, including turbidity, temperature and conductivity, was recorded continuously at 0.083 Hz (every 12 s) with two YSI6600 probes. One was located at 0.4 m above the bed and 3.9 m from the right bank, while the second probe was attached to a float and the sampling volume was located at 0.3 m below the water surface.

Further some laboratory experiments were conducted under controlled conditions using water and soil samples collected in the estuary. The relationships between acoustic backscatter strength and suspended sediment load were tested with the microADV system (Chanson et al., 2006). The data showed some monotonic functions between suspended sediment concentration (SSC) and acoustic backscatter intensity (BSI) (Fig. 4). The calibration data are shown in Fig. 4, where the backscatter intensity is defined as: $BSI = 10^{-5} \times 10^{0.043 \times Ampl}$ with Ampl the average signal amplitude in counts. The results were applied to the field study, and the data yielded a series of high-frequency long duration (50 Hz, 50 hours) measurements of turbulent velocity and suspended sediment concentration in

Fig. 3. Upper extent of Eprapah Creek estuary (riffles, Fig. 2) on 5–7 June 2006 looking upstream during dry and wet conditions. (A, Left) View from the right bank on 5 June 2006 at low tide – Note the absence of freshwater runoff, and the wooden debris. (B, Right) Photograph of the same section at low tide on 1 December 2005 after 130 mm of rain around midnight the night before, looking upstream – Note the strong freshwater runoff (flow from background to foreground), the high water level and the "brownish" colour of the flow highlighting suspended sediment runoff.
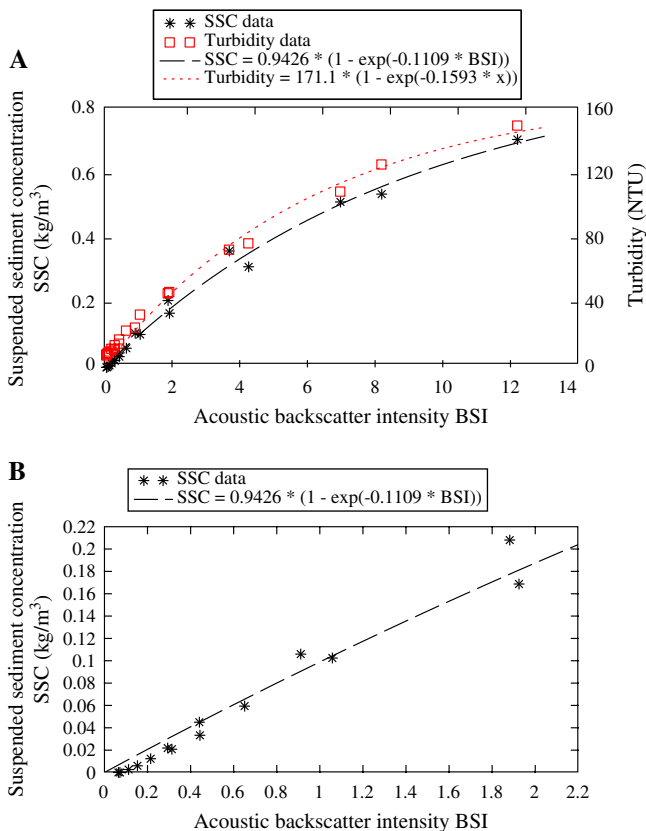

Fig. 4. Relationship between suspended sediment concentration and acoustic backscatter intensity for the Sontek 2D microADV (A641F) at Eprapah Creek. (A) Relationships between suspended sediment concentration, turbidity and acoustic backscatter intensity. (B) Detailed relationship between SSC and acoustic backscatter intensity for $0 \leq \text{SSC} \leq 0.2$ kg/m³.

the natural estuarine system. Note that the instantaneous suspended sediment concentration (SSC) was calculated for the post-processed backscatter amplitude data only. A preliminary data check showed a large number of signal amplitude "spikes/peaks" when the velocity data points that were deemed erroneous using the method of Chanson et al. (2005b). It is believed that these signal amplitude "spikes/peaks" might be caused by some electronic noises and inherent errors of the ADV system, rather than by some genuine suspended sediment clouds.

2.3. Calculations of turbulence properties

The post-processed data sets included the instantaneous velocity components V_x and V_y where x is the longitudinal direction positive downstream, and y is the transverse direction positive towards the left bank. A basic turbulence analysis yielded the first four statistical moments of each velocity component, their respective dissipative and integral time scales, as well as the tensor of instantaneous Reynolds stresses, and the first four statistical moments of the Reynolds stresses.

The turbulent velocity fluctuation is defined as: $v = V - \overline{V}$ where V is the instantaneous (measured) velocity component and $\overline{V}$ is the time average velocity component. When the flow is gradually time-variable, $\overline{V}$ is the low-pass filtered velocity component or variable-interval time average (VITA). Herein all turbulence data were processed using samples that contain 10,000 data points (200 s) and calculated every 10 s along the entire data set. The sample size (200 s) was deduced from a sensitivity analysis. It was chosen to be much larger than the instantaneous velocity fluctuation time scales, to contain enough data points to yield statistically stable and

meaningful results, and to be considerably smaller than the period of tidal fluctuations. In a study of boundary layer flows, Fransson et al. (2005) proposed a cut-off frequency that is consistent with the selected sample size.

An auto-correlation analysis yielded the Eulerian dissipation and integral time scales for each velocity component (Fig. 5) (Bradshaw, 1971; Piquet, 1999). The integral time scale, or Taylor macro scale, is a rough measure of the longest connection in the turbulent behaviour of a velocity component. The dissipation time scale represents a measure of the most rapid changes that occur in the fluctuations of a velocity component, and it is the smallest energetic time scale. Herein it was calculated using the method of Hallback et al. (1989) extended by Fransson et al. (2005) and Koch and Chanson (2005).

The Reynolds stress tensor includes the normal and tangential stresses. Each instantaneous Reynolds stress (e.g. $\rho v_x v_y$) is characterised by its first four statistical moments: i.e., the time-averaged stress $\rho \overline{v_x v_y}$, its standard deviation $(\rho v_x v_y)'$, skewness and kurtosis, where ρ is the fluid density.

The analysis of suspended sediment concentration (SSC) measurements yielded the first four statistical moments, and the integral time scale. All the calculations were performed using samples that contain 10,000 data points (200 s) and calculated every 10 s along the entire data sets.

Lastly the turbulence and SSC calculations were not conducted when more 20% of the 10,000 data points were corrupted/repaired during the ADV data post-processing.

3. Turbulence properties in the upper estuary

In the upper estuarine zone, the water depth and time-average longitudinal velocity were time-dependant and fluctuated with periods comparable to the tidal cycles and other large-scale processes. This is illustrated in Fig. 6 showing the water depth, water conductivity and time-averaged velocities measured at 3.1 km upstream of the river mouth. Fig. 6A presents the water depth and conductivity data. During a 24 h 50 min period, the water depth data showed two tidal cycles of slightly different periods and tidal ranges (Fig. 6A). The findings highlighted some slight tidal asymmetry, as well as some well-defined free-surface oscillations with periods about 3600 s. The water conductivity data showed some stratification between the bottom and the surface (Fig. 6A). The surface conductivity variations were driven primarily by the tides,

except at low tides. In shallow waters (less than 1 m), the water column was relatively well-mixed by turbulent mixing and the stratification observed at high tides disappeared as previously reported by Chanson (2003). Note the moderate range of specific conductivity that was typical of neap tide conditions in absence of freshwater runoff.

Fig. 6B presents the time-averaged longitudinal and transverse velocities recorded at 0.2 m above the bed, where the longitudinal velocity V_x is positive downstream towards the river mouth and the transverse velocity V_y is positive towards the left bank. The largest velocity magnitude was about mid-tides, but a major feature was the low-frequency oscillations of the longitudinal velocity with a period of 3600 s. These were noted particularly during the flood tide, high-tide slack and early ebb tide. These low-frequency oscillations were linked with the observed water depth fluctuations, and they are believed to result from some resonance caused by the tidal forcing interacting with the outer bay system (Moreton Bay). The writers observed some free-surface flow reversals around high tides and early ebb tides, with periods of between 11 and 14 min. These oscillations were linked with some form of internal resonance. Some similar, but smaller, low-frequency fluctuations were observed about mid-estuary of Eprapah Creek during neap tide conditions (Chanson, 2003; Trevethan et al., 2006).

3.1. Turbulence properties

The field observations showed systematically the large standard deviations of all velocity components during the flood tide and early ebb tide. Typical field measurements of standard deviations of the longitudinal velocity v'_x are shown in Fig. 7. Fig. 7 shows the magnitude of v'_x from a low water (LW1) to the next one (LW2), and the data are presented in a circular plot. The time variations of the data progress anti-clockwise, and the high waters are indicated also. Fig. 7 highlights the smaller velocity standard deviations during the end of the ebb tide, and the relatively large fluctuations in v'_x overall. The horizontal turbulence intensity v'_y/v'_x showed no discernable tidal trend, and v'_y/v'_x was equal to 0.44 in average. The value was comparable to laboratory observations in straight prismatic rectangular channels which yielded $v'_y/v'_x = 0.5$ to 0.7 (Nezu and Nakagawa, 1993; Koch and Chanson, 2005).

The tangential Reynolds stress $\rho \overline{v_x v_y}$ varied very slightly with the tide during the field work. Fig. 8A illustrates the trend
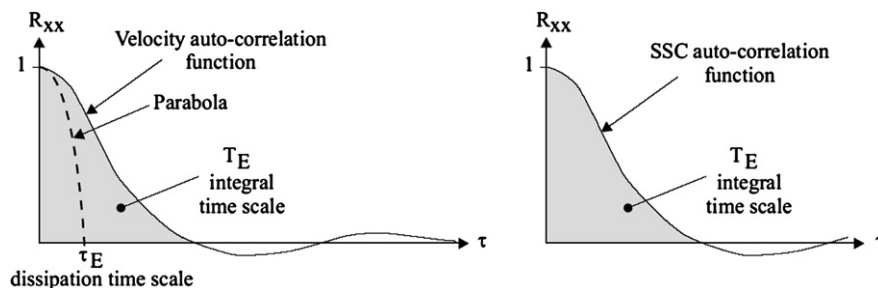

Fig. 5. Definition sketches of velocity auto-correlation function and turbulent time scales, and of suspended sediment concentration auto-correlation function.
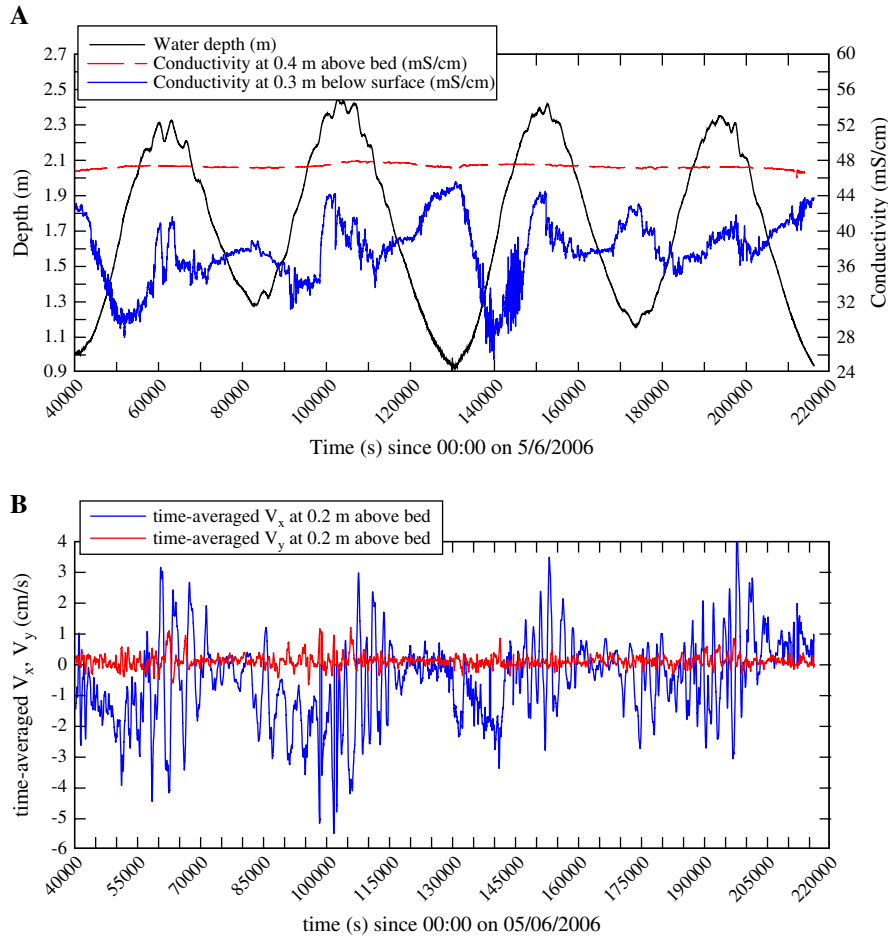
Fig. 6. Measured water depth, water conductivity and time-averaged velocities during the field work E7 on 5−7 June 2006 (neap tide conditions). (A) Measured water depth (m) and water conductivities (mS/cm). (B) Time-averaged streamwise and transverse velocity data at 0.2 m above bed − Time-averages calculated for 10,000 data points every 10 s along data set.

for the entire field study by showing the time-averaged Reynolds stress $\rho\overline{v_x v_y}$ as a function of time-averaged longitudinal velocity $\overline{V_x}$. $\rho\overline{v_x v_y}$ was predominantly positive during the flood tide and negative during the ebb tide (Fig. 8A), and the data were correlated by:

$$\rho\overline{v_x v_y} = -4.03 \times 10^{-7}\, \overline{V_x} \tag{1}$$

where $\rho\overline{v_x v_y}$ and V_x are in Pa and m/s respectively. The standard deviations of tangential Reynolds stresses tended to increase with increasing flow velocity magnitude, but the data
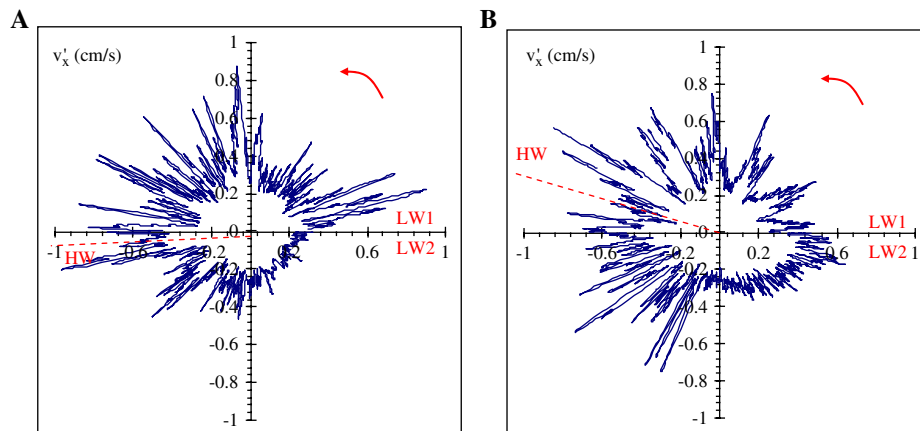

Fig. 7. Standard deviations of longitudinal velocity v'_x (cm/s) during two consecutive tidal cycles. (A) $t = 39,660$ (LW1) to 83,280 (LW2) s, max. tidal range: 1.07 m. (B) $t = 83,280$ (LW1) to 128,880 (LW2) s, max. tidal range: 1.39 m.
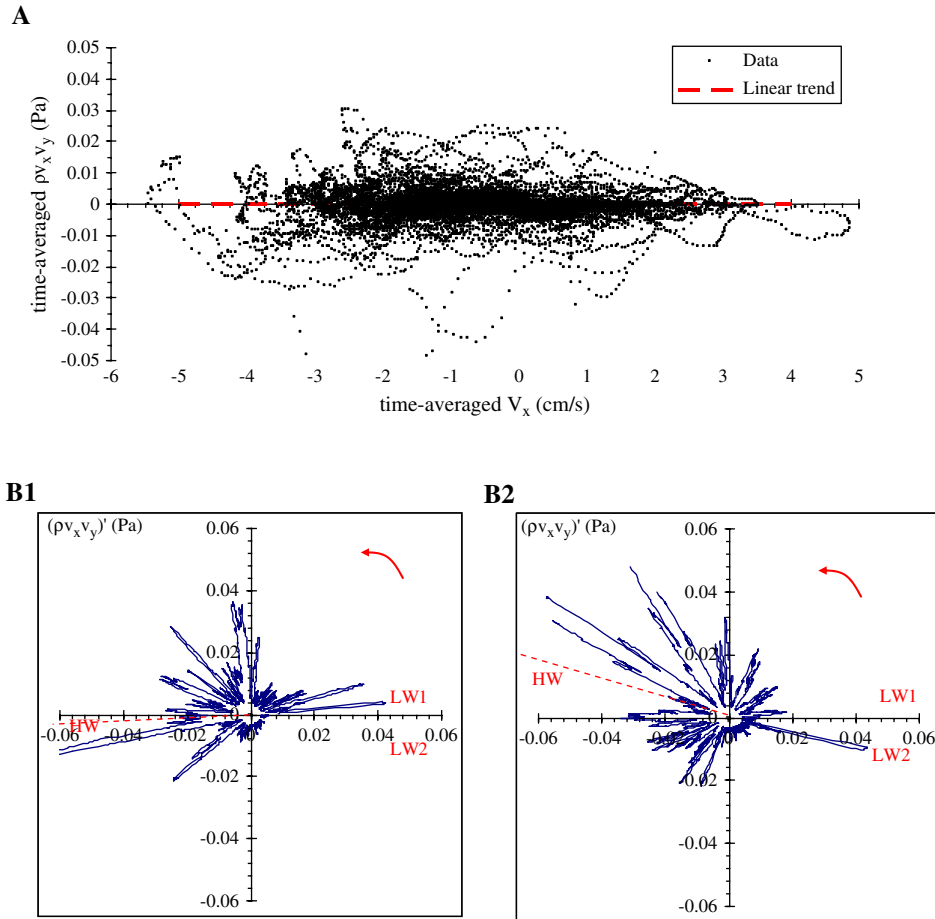
A

B1

B2

Fig. 8. Tangential Reynolds stress $\rho v_x v_y$ (Pa) calculated for 10,000 data points every 10 s along the entire data set. (A) Time-averaged Reynolds stress $\rho\overline{v_x v_y}$ as a function of time-averaged streamwise velocity. (B) Standard deviations of tangential Reynolds stress during two consecutive tidal cycles. (B1) $t = 39,660$ (LW1) to 83,280 (LW2) s, max. tidal range: 1.07 m. (B2) $t = 83,280$ (LW1) to 128,880 (LW2) s, max. tidal range: 1.39 m.

showed very significant fluctuations (Fig. 8B). Fig. 8B presents some data for two consecutive tidal cycles. In average, the dimensionless tangential stress fluctuation $(v_y v_x)'/(v_y' v_x')$ was 1.3 for the entire study. For comparison, some laboratory observations in a straight prismatic rectangular channel yielded $(v_y v_x)'/(v_y' v_x') \sim 1.0$ to 1.6 (Koch and Chanson, 2005). The present results demonstrated further that the probability distribution functions of the tangential Reynolds stress $\rho v_x v_y$ were not Gaussian.

3.2. Turbulent time scales

Some time-variations of the integral time scales T_{Ex} and T_{Ey} are shown in Fig. 9 for a tidal cycle. Note that the axes have a logarithmic scale and the units are milliseconds. The integral time scales of streamwise velocity T_{Ex} were significantly larger during the flood tide than during the ebb tide (Fig. 9A). The horizontal integral time scales T_{Ex} and T_{Ey} were typically between 0.07 and 0.8 s, and 0.5 and 1.5 s respectively at 0.2 m above the bed. The dimensionless integral time scale T_{Ey}/T_{Ex} was about 3.6 in average. In two tidal systems in Australia, Osonphasop (1983) and Trevethan et al. (2006) observed respectively $T_{Ey}/T_{Ex} \sim 1.7$ and 1.0 in a tidal

channel and mid-estuary respectively, while Koch and Chanson (2005) observed $T_{Ey}/T_{Ex} \sim 0.4$ in a laboratory channel.

The analysis of dissipation time scales of all velocity components showed no obvious trend with the tidal phase (Fig. 10). The turbulent dissipation time scale, or Taylor micro-scale, is a characteristic time scale of the smaller eddies which are primary responsible for the dissipation of energy. The data yielded dissipation time scales of about 1 ms in average, with most data between 0.0004 and 0.003 s. Such dissipation time scales were smaller than the time between two consecutive samples: e.g., $1/F_{scan} = 0.02$ s for $F_{scan} = 50$ Hz. The findings highlighted that a high-frequency sampling is required and the sampling rates must be at least 50 Hz to capture a range of eddy time scales relevant to the dissipation processes. The dimensionless transverse dissipation time scale was about $\tau_{Ey}/\tau_{Ex} \sim 1.9$. Koch and Chanson (2005) obtained $\tau_{Ey}/\tau_{Ex} \sim 0.9$ in a rectangular channel.

Some estimates of integral length scales may be derived using Taylor's hypothesis. If the transport by advection and diffusion are assumed two separate additive processes, the integral turbulent length scale may be estimated as: $\Lambda_f = \overline{V_x} T_E$. The integral length scale Λ_f is a measure of the longest connection between the velocities at two points of the flow
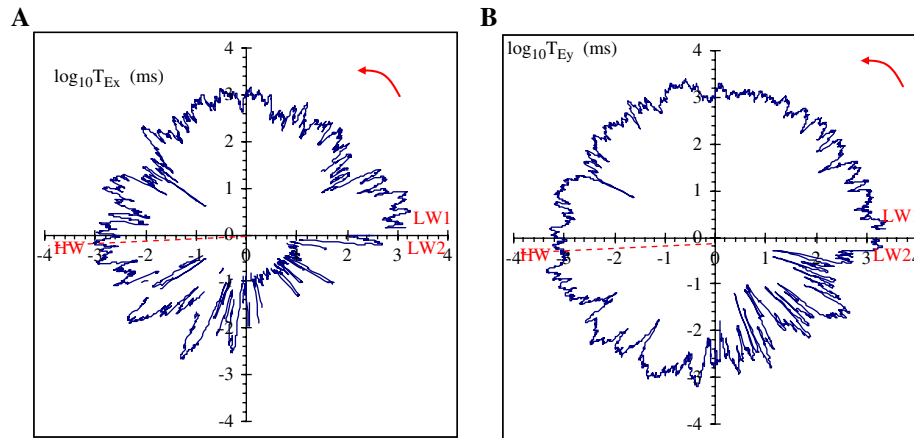
A

B

Fig. 9. Integral turbulent time scales (units: ms) – Note the logarithmic scale of the axes. (A) Longitudinal integral time scales T_{Ex} for $t = 39,660$ (LW1) to $83,280$ (LW2) s. (B) Transverse integral time scales T_{Ey} for $t = 39,660$ (LW1) to $83,280$ (LW2) s.

field (Hinze, 1975). In the present study, the horizontal integral length scales were between 0.2 and 3 cm.

4. Time-variations of suspended sediment concentration

The time variations of instantaneous suspended sediment concentration (SSC) showed some fluctuations throughout the entire field study, including during the tidal slacks (high and low tides). This is illustrated in Fig. 11 showing the time-variations of the time-averaged SSC and of its standard deviations. The data tended to indicate also larger suspended loads during the early flood tides: e.g., $t = 40,000$ to $52,000$ s and $130,000$ to $140,000$ s (Fig. 11). The writers noted also some low-frequency oscillation patterns that may be linked with the low-frequency fluctuations of streamwise velocity. For the field study, the ratio $SSC'/\overline{SSC}$ was about 0.57 in average.

The instantaneous advective suspended sediment flux per unit area q_s was calculated as:

$$q_s = SSC \, V_x \qquad (2)$$

where q_s and V_x are positive in the downstream direction, and the suspended sediment concentration SSC is in kg/m³. The instantaneous suspended sediment flux per unit area results are presented in Fig. 12. Note that the data characterise the advective suspended sediment flux per unit area at the ADV sampling volume location 0.2 m above the bed only. The sediment flux per unit area data showed typically an upstream, negative suspended sediment flux during the flood tide and a downstream, positive sediment flux during the ebb tide. The instantaneous suspended sediment flux per unit area data q_s showed considerable time-fluctuations that derived from a combination of velocity and suspended sediment concentration fluctuations. The data demonstrated further some high-frequency fluctuation with some form of suspended sediment flux bursts that were likely linked to and caused by some turbulent bursting phenomena next to the bed (e.g. Jackson, 1976). Some low-frequency fluctuations in suspended sediment flux were also observed.
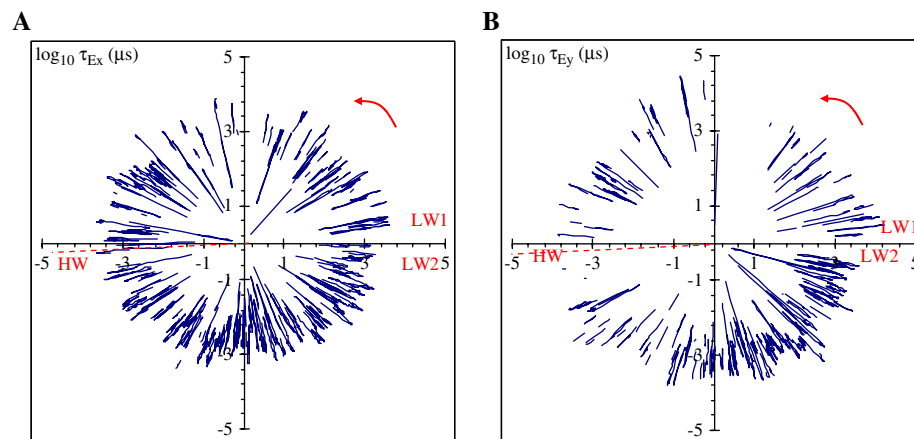
A

B

Fig. 10. Turbulent dissipation time scales (units: microseconds) – Note the logarithmic scale of axes. (A) τ_{Ex} for $t = 39,660$ (LW1) to $83,280$ (LW2) s. (B) τ_{Ey} for $t = 39,660$ (LW1) to $83,280$ (LW2) s.
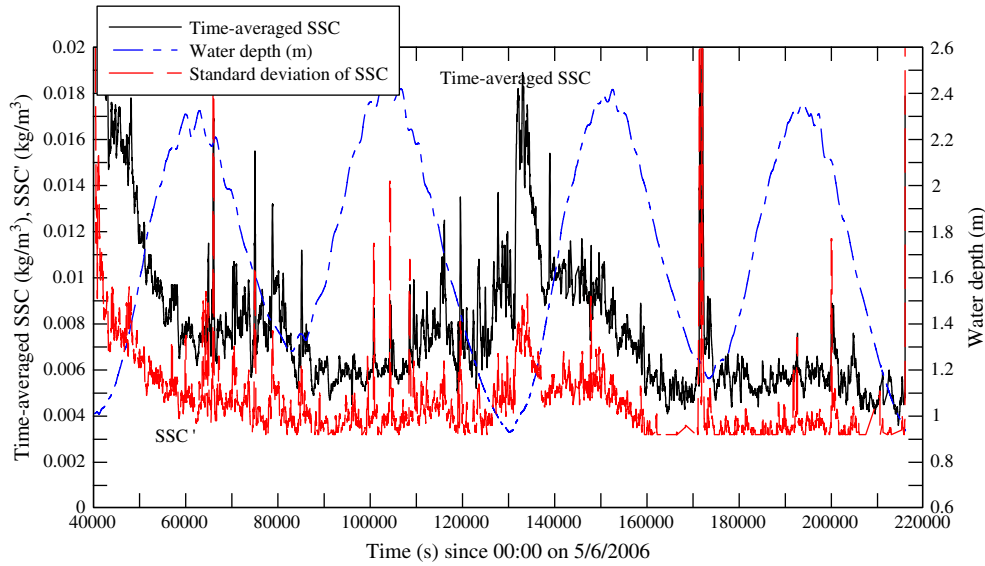
Fig. 11. Time variations of the time-averaged suspended sediment concentration and of the standard deviation of SSC, as well as measured water depth, for the 50 hours study period.

4.1. Suspended sediment concentration time scales

The integral time scale of the suspended sediment concentration (SSC) data represents a characteristic time of turbid suspensions in the creek. Typical results are presented in Fig. 13 for two cycles during the field study. Note that the axes have a logarithmic scale and the units are milliseconds. Overall the SSC integral time scale data seemed independent of the tidal phase (Fig. 13). They yielded SSC′s integral time scales between about 0.04 and 0.2 s for the study.

A comparison between turbulent and SSC integral time scales showed some difference especially during the ebb tide. For example, consider Figs. 9 and 13A which correspond to the same period. For the entire study, the ratio of SSC to turbulent integral time scales was about: $T_{E_{SSC}}/T_{Ex} \sim 1$ and 0.18 during the flood and ebb tides respectively. The contrasted finding might suggest that the suspended sediment concentrations were dominated by turbulent processes during the flood tide, but not during the ebb tide. The experimental results

showed further some significant fluctuations in SSC integral time scales during the tidal cycle.

Some estimates of integral SSC length scales may be derived from Taylor's hypothesis. In the present study, the integral length scales for sediment suspension were between 0.05 and 0.2 cm.

4.2. Discussion

For each tidal cycle (24 h 50 min) of the study, the suspended sediment flux per unit area data were integrated with respect of time. The results gave the net sediment mass transfer per unit area at the ADV sampling volume located 0.2 m above the bed:

$$m_s = \int_{24\,h\,50\,min} SSC\,V_x\,dt \tag{3}$$

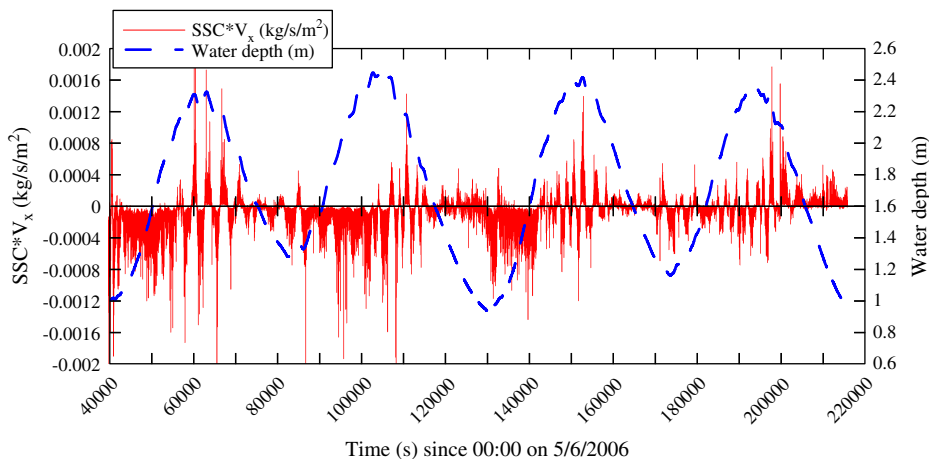Fig. 12. Time variations of suspended sediment flux per unit surface area (SSC V_x, positive downstream) and measured water depth for the 50 hours study period.
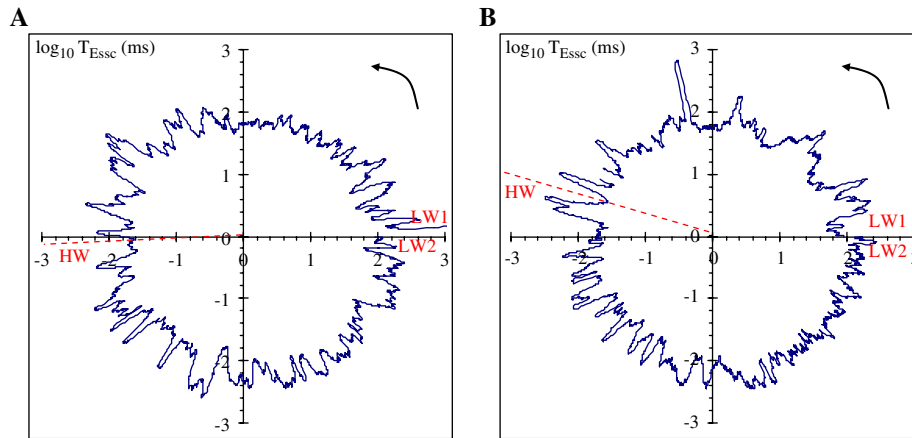
Fig. 13. Suspended sediment concentration (SSC) integral time scales (units: milliseconds) − Note the logarithmic scale of axes. (A) Longitudinal integral time scales T_{Essc} for $t = 39,660$ (LW1) to 83,280 (LW2) s, max. tidal range: 1.07 m. (B) Transverse integral time scales T_{Essc} for 83,280 (LW1) to 128,880 (LW2) s, max. tidal range: 1.39 m.

The net sediment mass transfer per area was negative (i.e. up-stream). Eq. (3) yielded $m_s = -6.66$ and -1.81 kg/m^2 for each tidal cycle.

5. Conclusion

In natural estuaries, the suspended sediment processes are driven by the turbulent momentum mixing. Herein detailed turbulence and suspended sediment field measurements were conducted simultaneously and continuously at high frequency in a small subtropical estuary with semi-diurnal tides. The study was focused on the upper estuarine region of this elongated tidal creek. The data set demonstrated some unique features of the upper estuary, in particular some low-frequency longitudinal flow oscillations induced by internal and outer resonance. The probability distribution functions of the velocity components and of the tangential Reynolds stress $\rho v_x v_y$ were not Gaussian. The integral time scales for turbulence and suspended sediment concentration were about equal during flood tides, but differed significantly during ebb tides.

A striking feature of the data sets is the large fluctuations in all turbulence characteristics and of the suspended sediment concentrations during the tidal cycle. This feature has been rarely documented. But an important difference between this study and earlier measurements is that the present data were collected continuously at high frequency during a relatively long period.

References

Bradshaw, P., 1971. An Introduction to Turbulence and its Measurement. Pergamon Press, Oxford, UK (The Commonwealth and International Library of Science and Technology Engineering and Liberal Studies Thermodynamics and Fluid Mechanics Division, 218 pp.).

Chanson, H., 2003. A Hydraulic, Environmental and Ecological Assessment of a Sub-tropical Stream in Eastern Australia: Eprapah Creek, Victoria Point QLD on 4 April 2003. Report No. CH52/03. Dept. of Civil Engineering, The University of Queensland, Brisbane, Australia, June, 189 pp.

Chanson, H., Brown, R., Ferris, J., Ramsay, I., Warburton, K., 2005a. Preliminary measurements of turbulence and environmental parameters in a sub-tropical estuary of eastern Australia. Environmental Fluid Mechanics 5 (6), 553–575.

Chanson, H., Trevethan, M., Aoki, S., 2005b. Acoustic Doppler velocimetry (ADV) in small estuarine system. In: Jun, B.H., Lee, S.I., Seo, I.W., Choi, G.W. (Eds.), Field Experience and "Despiking". Proc. 31st Biennial IAHR Congress, Seoul, Korea, pp. 3954–3966 (Theme E2, Paper 0161).

Chanson, H., Takeuchi, M., Trevethan, M., 2006. Using Turbidity and Acoustic Backscatter Intensity as Surrogate Measures of Suspended Sediment Concentration. Application to a Sub-Tropical Estuary (Eprapah Creek). Report No. CH60/06. Div. of Civil Engineering, The University of Queensland, Brisbane, Australia, August, 44 pp.

Digby, M.J., Saenger, P., Whelan, M.B., McConchie, D., Eyre, B., Holmes, N., Bucher, D., 1999. A Physical Classification of Australian Estuaries. Report No. 9, LWRRDC. National River Health Program, Urban Sub-Program. Occasional Paper, 16/99.

Fransson, J.H.M., Matsubara, M., Alfredsson, P.H., 2005. Transition induced by free-stream turbulence. Journal of Fluid Mechanics 527, 1–25.

Goring, D.G., Nikora, V.I., 2002. Despiking acoustic Doppler velocimeter data. Journal of Hydraulic Engineering. ASCE 128 (1), 117–126. Discussion: 129 (6), 484–489.

Hallback, M., Groth, J., Johansson, A.V., 1989. A Reynolds Stress Closure for the Dissipation in Anisotropic Turbulent Flows. Proc. Seventh Symp. Turbulent Shear Flows, vol. 2. Stanford University, USA, pp. 17.2.1–17.2.6.

Hinze, J.O., 1975. Turbulence, second ed. McGraw-Hill, New York, USA.

Jackson, R.G., 1976. Sedimentological and fluid-dynamic implications of the turbulent bursting phenomenon in geophysical flows. Journal of Fluid Mechanics 77 (Pt 3), 531–560.

Koch, C., Chanson, H., 2005. An Experimental Study of Tidal Bores and Positive Surges: Hydrodynamics and Turbulence of the Bore Front. Report No. CH56/05. Dept. of Civil Engineering, The University of Queensland, Brisbane, Australia, July, 170 pp.

Nezu, I., Nakagawa, H., 1993. Turbulence in Open-Channel Flows. IAHR Monograph, IAHR Fluid Mechanics Section. Balkema Publ., Rotterdam, The Netherlands, 281 pp.

Osonphasop, C., 1983. The Measurements of Turbulence in Tidal Currents. Ph.D. thesis, Dept of Mech. Eng., Monash Univ., Australia.

Piquet, J., 1999. Turbulent Flows. Models and Physics. Springer, Berlin, Germany, 761 pp.

Trevethan, M., Chanson, H., Brown, R.J., 2006. Two Series of Detailed Turbulence Measurements in a Small Subtropical Estuarine System. Report No. CH58/06. Div. of Civil Engineering, The University of Queensland, Brisbane, Australia, March, 153 pp.